Lateral Reynolds Stress and Eddy Viscosity in a Coastal Strait

KEIR COLBO*

School of Earth and Ocean Sciences, University of Victoria, Victoria, British Columbia, Canada

(Manuscript received 30 March 2004, in final form 4 August 2005)

ABSTRACT

The lateral Reynolds stress $\overline{uv}$, representing the transfer of along-strait momentum toward the sides of Juan de Fuca Strait, is measured with an array of ADCPs. The contributions to the stress from a number of frequency bands are analyzed to highlight the roles of different processes. Motion in a frequency band that includes internal waves and Doppler-shifted subinertial eddies gives a Reynolds stress that, when scaled by the observed shear, is consistent with an eddy viscosity of $O(10\ \mathrm{m^2\ s^{-1}})$. This viscosity acts on the tides and the estuarine flow. The tides can also impart a viscous stress upon the low-frequency estuarine flow. These tidal currents, although strong, are largely nondivergent within the area of the array and thus appear to be less important for the cross-strait transfer of momentum. The long-term mean estuarine circulation can be acted upon by meanders of the estuarine flow, defined as features with periods of 3–5 days. These meanders are found to also have a horizontal eddy viscosity of $O(10\ \mathrm{m^2\ s^{-1}})$. The measured Reynolds stress divergences are consistent with both the strongly curved profile of the estuarine mean flow and also the more slablike tidal current profile. This paper represents the first direct calculation of eddy viscosity on the medium-sized scale of the array, $O(1\ \mathrm{km})$.

1. Introduction

The lateral transfer of momentum in the ocean has received only limited attention. In the deep ocean, away from fronts, the gradients of velocity are quite small and thus the lateral transfer of momentum may be of secondary importance. However, in the coastal environment, there are large gradients in the horizontal velocity field because of the no-slip condition at the boundaries. Moreover, if the stratification is such as to severely limit vertical mixing, then horizontal fluxes may be the primary source of friction. This lateral transport of momentum needs to be included for the correct modeling of coastal dynamics for use in shipping, pollution control, fishing, and recreational boating.

Horizontal gradients in velocity can be because of horizontal gradients in the energy sinks acting on the flow. Edwards et al. (2004) have discussed the role of form drag in extracting energy from the barotropic tide. In the location of their observations, Three Tree Point, Washington, they found that the internal drag resulting from the generation of eddies and internal lee waves was a significant multiple of the drag resulting from the frictional bottom boundary layer. Thorpe (1992) found, in a numerical model, that the form drag was approximately equal to the frictional drag. Form drag is likely to be an important process in coastal waters because it both transfers energy from the large-scale flow into eddies and internal waves, and sets up horizontal shears. However, we need to understand the horizontal stresses acting on this flow to predict its time evolution.

In particular, fully developed flow in a channel, with constant eddy viscosity, has a well-known parabolic profile. However, for many geophysical flows the channel length may be too short to allow the turbulent boundary layers on the two sides to grow into the middle of the channel. In this case the flow profile will be slablike, with the shear located only near the boundaries. For a given geometry, the choice of whether the flow profile will be slablike or parabolic is dependent on the eddy viscosity and its cross-strait profile.

There are no other calculations of lateral Reynolds stress divergence, or horizontal eddy viscosity, based

* Current affiliation: Physical Oceanography Department, Woods Hole Oceanographic Institution, Woods Hole, Massachusetts.

Corresponding author address: Dr. Keir Colbo, Woods Hole Oceanographic Institution, Physical Oceanography Dept., MS 29, Woods Hole, MA 02543.
E-mail: kcolbo@whoi.edu

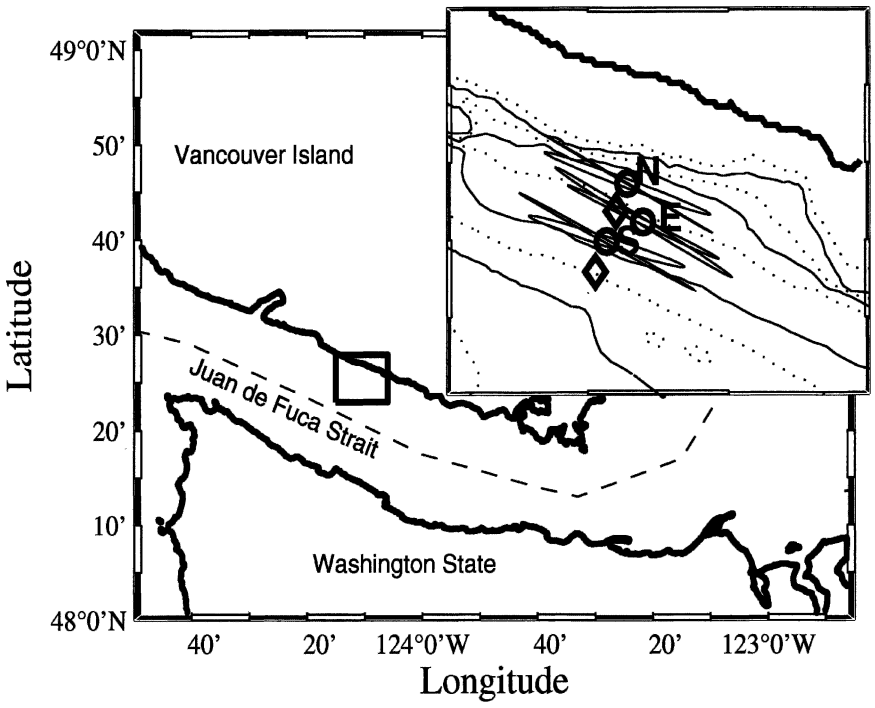

FIG. 1. Juan de Fuca Strait with the region of mooring work indicated by the rectangle. The inset shows the mooring array with ADCPs (circle) and temperature chain moorings (diamonds). The contours represent the bathymetry in 20-m intervals. Superimposed on the ADCP moorings are M_2 tidal ellipses from 10 m above the bottom and 20 m below the surface.

upon observations on the scale of hundreds of meters to several kilometers. These are the typical scales of the coastal ocean computer models that need a parameterization for eddy viscosity. The only comparison is with eddy diffusivity, not eddy viscosity, deduced from the spread of dye during the Coastal Mixing and Optics Experiment (Sundermeyer and Ledwell 2001). Aside from the fact that they measure diffusivity, the value Sundermeyer and Ledwell (2001) obtain is the result of averaging over the whole experiment, and so it includes numerous processes that occur at vastly different time scales.

In this paper, we report on lateral Reynolds stress calculations made from observations taken in Juan de Fuca Strait. Juan de Fuca Strait is a long, deep body of water that lies between Vancouver Island, Canada, and the Olympic Peninsula of Washington State (Fig. 1). It possesses the advantages of fairly uniform bathymetry, strong stratification (Fig. 2), and substantial currents. The regularity of the bottom topography is important because it limits the complications resulting from flow curvature. The strong stratification when coupled with the relatively deep bathymetry is important because it implies that the majority of the water column is outside of a thin bottom boundary layer (Ott 2000), and is therefore not routinely mixed by the tidal currents. The strong tidal currents are important because they provide the energy to support an energetic internal wave and small-scale eddy field.

The cross-strait profile of the along-strait current exhibits two markedly different shapes depending on the type of flow studied. The mean estuarine flow during the summer months exhibits a markedly curved, as opposed to slablike, cross-strait profile (Labrecque et al. 1994; Masson and Cummins 2000). On the other hand, the tidal velocity, although observed to have large gradients very near the boundaries (Colbo 2002), is much more uniform in its cross-strait profile (Foreman et al. 1995). In this paper, we seek to explain these differences by quantifying the lateral Reynolds stress ($\overline{uv}$) that transfers the momentum of the flow toward the boundaries where it can be lost. Because we measure the velocity field at a number of locations, we obtain not just the stress but also its divergence. The horizontal shear of the large-scale flow is also calculated, and thus we can formulate an appropriate eddy viscosity A_H.

2. Background and observations

During the summer months, Juan de Fuca Strait exhibits a classic estuarine flow with strong outflow on the

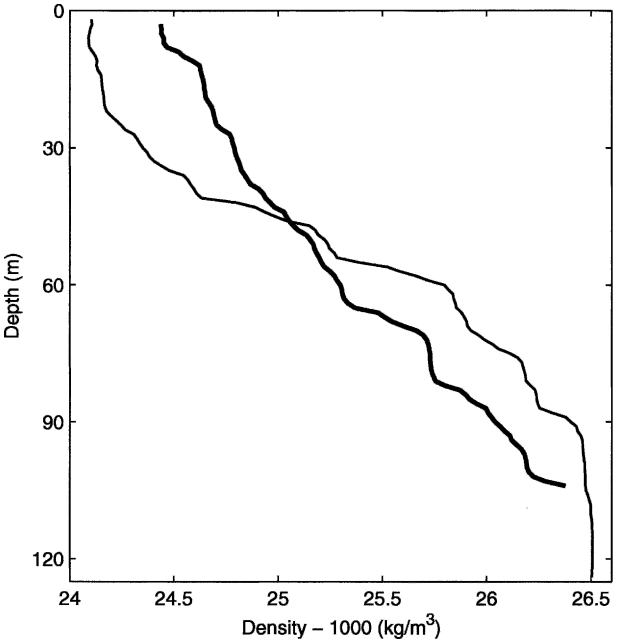

FIG. 2. Two CTD profiles obtained from within 1 km of the mooring array. The two were taken 13 days apart and show the variability introduced by the spring–neap cycle (strongest stratification occurs 2–3 days after spring tides).

surface and a weaker return flow underneath. The system is forced primarily by the Fraser River. The peak freshet resulting from snowmelt is about 8000 $m^3 s^{-1}$ in late June, and this represents about 50% of the freshwater entering Juan de Fuca Strait. Average summer stratification is strong ($N \sim 0.016$ s^{-1}). Juan de Fuca Strait is also wide enough to feel the effects of rotation such that the lighter outflowing water tends to hug the northern side of the strait, while the denser inflow is concentrated on the southern side. The zero velocity isotach is very shallow (<10 m depth) along the southern coast and deepens as one progresses north across Juan de Fuca Strait such that it intersects the bottom at a depth of ≈100 m, several kilometers from the northern boundary. Our data are from the northern section of Juan de Fuca Strait where the mean flow is primarily directed out to sea.

Historical data from Juan de Fuca Strait consist of some sparsely located point current meters located in cross-strait lines (Labrecque et al. 1994). These data, as mentioned above, show that the mean cross-strait profile during the summer months is quite curved. Instead of attempting to instrument a complete cross-strait transect, we have concentrated on deploying a small array of acoustic Doppler current profilers (ADCPs) near the northern boundary. This allowed us to resolve the gradients in the Reynolds stress near the side boundary. The data were collected in June–August 1999 during the time of peak runoff and consisted of the records from three bottom-mounted upward-looking 30-kHz ADCP moorings and two temperature chain moorings (Fig. 1).

Although the ADCPs are not aligned on a single cross-channel transect, we shall assume that variations in the statistics of the flow in the along-strait direction are negligible over the spacing of the moorings, O(700 m). The north and south ADCPs were deployed for 51 days while the east ADCP was only added for the last 31 days. We shall thus constrain our analysis to the period when all three ADCPs were in the water. Two temperature chains that were instrumented with individual, internally recording temperature pods, spaced between 5 and 10 m apart, were deployed nearby. Most of the instruments only recorded temperature, but we also had two temperature–conductivity pods and two temperature–pressure pods on each mooring. The temperature chains also had two S4 current meters located approximately 15 m below the surface and 6 m above the bottom. In this paper, I shall only make use of the temperature chain data as a means to map the results between the different ADCP moorings, by comparing the Reynolds stresses along isothermal (a reasonable proxy for isopycnal over the scale of the array) surfaces, which may occur at different depths at different moorings. Some specifics of the moorings are presented in Table 1. The offshore distance is the distance, not from the shoreline, but rather from the 20-m isobath, which represents the shallow side of the steep topography to the north of the mooring array (Fig. 1). This attempts to exclude the broad, shallow shelf near the northern coast in the region of our mooring array. Because we have no obvious manner in which to estimate the lateral Reynolds stress along this 20-m isobath, we shall restrict estimates of eddy viscosity (based upon stress differences) to below this depth.

The calculation of a Reynolds stress is based upon an arbitrary distinction between the mean and the fluctuations. We shall select several different choices of the mean and the fluctuations in order to focus on particu-

TABLE 1. Specifics of the mooring setups.

	Water depth (m)	Depth resolution (m)	Time resolution (s)	Offshore distance (km)
South ADCP	112	1	120	1.8
East ADCP	100	2	120	1.0
North ADCP	77	1	60	0.35
T chain south	129	5–10	20–300	2.5
T chain north	102	5–10	20–300	1.0

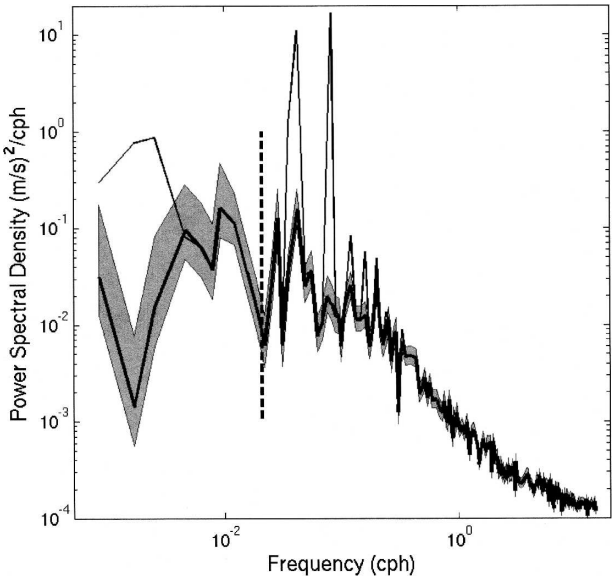

FIG. 3. Spectra of the along-isobath component of velocity from 50-m depth at the south ADCP mooring. The thin line represents the original spectra, and the thick line (with shaded 90% confidence limits) is the spectra after detiding. The vertical dashed line is the cutoff frequency between the internal wave–eddy band and the meander band.

lar processes. The velocity field will be decomposed into four bands. In order of decreasing frequency they are as follows: the internal wave–eddy field, the tidal currents, the meanders of the estuarine flow, and the long-term mean estuarine flow. Two of these components of velocity are straightforward. The tidal current is determined by a harmonic analysis (Foreman 1978), and the long-term mean estuarine flow is simply the mean over the length of the observations. The other two components are determined by a partitioning of the residual currents. Everything with a frequency higher than 1/2 cycle per day (cpd) is in the internal wave–eddy band and everything with a frequency less is in the meander band. This partitioning is rather crude, but the choice of 1/2 cpd is based upon the distinct lack of kinetic energy at this frequency (Fig. 3). The internal wave–eddy field band thus consists of all of the internal waves plus a component resulting from small eddies, O(1–2 km), that can be Doppler shifted by the tidal flow into this observed frequency range. These eddies are formed by interaction between the tidal currents and the irregular coastline (Edwards et al. 2004). The meanders are less well resolved in terms of a single process, but could be because of baroclinic instabilities of the sloping estuarine mean flow.

Given this decomposition of the current, one can then proceed to look at how the higher-frequency fluctuations act to transport momentum in the reference frame of the lower-frequency mean. Except for the internal wave–eddy field band, which overlaps the tidal band, there is a clear spectral gap between each of our four components. For the specific case of the internal wave–eddy field acting as fluctuations in transporting the momentum of the tidal current, we will need to ensemble average over many similar "phases" of the tide to get robust statistics.

a. ADCP data

The ADCP horizontal velocity data were uniformly excellent, except for occasional drops in signal strength near the surface (upper 15 m) during daylight hours. This change in near-surface backscatter intensity is related to the diel migration of zooplankton, and indicates that the near-surface water column is largely void of scatterers during the day (Ott 2000). Many of the velocities that do exist during daylight hours in this near-surface region are the result of three-beam solutions and are less believable. Our ADCPs were programmed such that they see the surface reflection. However, sidelobe contamination generally invalidates the signal in the top 6% of the water column for our 20° beam spread. Thus, we lose the velocity signal in the top 5–7 m, depending on the ADCP.

The ADCP was programmed to perform a burst of pings, typically 15 over 15 s, and then average the resulting velocities. This allows for an improved estimate of the beam velocity for any feature that is stationary over the period of sampling. The standard Teledyne RD Instruments, Inc., (RDI) formula for our sampling strategy would predict an rms error in the velocity of 1.5 cm s^{-1}. Assuming the errors are uncorrelated, then the introduced error in our Reynolds stress calculation is $<0.5 \times 10^{-5}$ m^2 s^{-2} for the stresses calculated in section 3a. It would be even less for the later sections, which involve significantly more averaging.

The tides play an important role in the dynamics of Juan de Fuca Strait. They represent both a large component of the observed velocity and act as a forcing for other motions, such as internal waves and eddies. We therefore would like to identify the tidal motion within the total velocity field and thus be able to separate the total velocity into tidal and residual components. Luckily, the tides are well-behaved, regular phenomena with known frequencies for the different astronomical components. We separate the tides by fitting sinusoids with known tidal frequencies to the data. The standard tidal analysis package of Foreman (1978) is used to perform this decomposition separately at each depth bin and for each ADCP. The resulting output provides major and minor axis amplitudes plus inclinations and phases for all of the resolved components. A Rayleigh criterion of

0.8 is used and we deduce the ratio and phase of undetermined constituents (i.e., P_1 vs K_1 and K_2 vs S_2) from previous nearby long-term records.

Figure 1 shows the M_2 tidal ellipses at 20 m above the bottom and 20 m below the surface for each of the moorings. They all show similar behavior. The ellipses near the bottom are closely aligned with the topography, whereas the near-surface ones are rotated slightly clockwise. In examining the full water column we see that ellipses are largely along isobaths from above the bottom boundary layer to about 30-m depth. Above this the tidal ellipses veer to follow a direction more closely aligned with the coast.

b. Temperature chain data

The individual temperature pods that comprised the temperature chain moorings suffered from several data problems. It was discovered that some of the temperature pods would intermittently switch off for exactly 1-day periods. They also all suffered some degree of clock drift. After each individual temperature record was reset to a correct time axis, and the breaks in the record were identified (usually with the help of nearby pods), we used a mooring motion program (Dewey 1999) to correct for the laying over of the taut-wire mooring in the strong currents, although the maximum change in depth was <3 m for the temperature chains. At each temperature chain mooring we now have a time–depth matrix of temperature spanning the water column from 5 m above the bottom to 15 m below the surface.

Although we developed a temperature–salinity (T–S) mapping procedure for studying consistency relations, for the simple problem of mapping between moorings we can get by with just temperature instead of density, because T–S properties do not change significantly over the scale of the array.

The temperature chain moorings are not located on top of the ADCPs, so we need to make some assumptions about how the isopycnal structure changes in the cross-strait direction (the y axis in our coordinate system). Based upon CTD measurements over several years in this region, the isopycnal surfaces generally slope down to the north at a constant angle (away from the surface layer). We thus calculate the slope of the temperature surfaces between the north and south T chains and project this slope northward to the location of the north ADCP. ADCP bins are then compared along these surfaces. In principle, the isopycnal slopes are quite weak, $O(1/500)$, and so the mapping is not greatly different from a constant depth comparison.

3. Data analysis

The Reynolds stress is critically dependent on both the choice of orientation of the axes, and on the length of the time window used in the averaging. Furthermore, the Reynolds stress divergence, not the stress itself, is the dynamically interesting quantity. Because we wish to calculate the stress divergence between moorings and relate the stress to an eddy viscosity, we need to pick a consistent orientation for the axes used at the three moorings. Note that we do not need to choose a single axis orientation to represent all density surfaces, but we could instead have one that varies with height and is projected to the other moorings along an isopycnal surface.

In principle our methods are always very similar. We first choose a time window over which to perform the averaging, based upon some physical understanding of the processes we are trying to resolve. The average direction of the "mean" flow during that window is calculated and represents the orientation of the x axis. The "fluctuations" are then rotated into the chosen axis, and the product of the u and v components gives an estimate of the Reynolds stress.

a. Reynolds stresses acting on the tidal current

We start with a calculation of the effect of the internal wave–eddy field in transferring the momentum of the tidal current. Because there is no spectral gap between these two processes, we will need to ensemble average the Reynolds stresses over many realizations, each of which should represent similar tidal conditions.

1) CHOOSING THE TIME WINDOW

The time window over which we calculate the Reynolds stress is limited by two factors. The first is that it should be short enough such that the tidal current is approximately constant during the window, and hence represents a mean state. The second is that a longer window averages over more of the internal wave–eddy band and gives better statistics. As a first estimate we shall use a 1-h window to calculate the stresses.

There might be sensitivity to the choice of a 1-h averaging window. We tested this by replacing the 1-h window with windows of either 30 min or 2 h and comparing the results. In general, the Reynolds stress was only mildly sensitive to the length of averaging window. There are two explanations for this lack of sensitivity. The first is that there is a spectral gap between the tides and the fluctuations, such that we realize there are several periods of fluctuation in each averaging window. We know that there is no spectral gap.

The second explanation is that the dominant processes are longer than our time window and so each time average is not much better than a point measurement. Comparing the Reynolds stresses between ensemble members at a given phase of the tide, we see that there is large variability that only becomes significant because of our long record lengths. This points to the second explanation where the dominant process is much longer than our 1-h window. It would also explain why the variance among ensemble members varies inversely with the size of the time window. We thus feel that a 1-h time window is a reasonable compromise.

2) CHOOSING THE AXES ORIENTATION

There are several sensible choices for the Reynolds stress axis. The first would be to align the axis with the local bathymetry in the neighborhood of the moorings. A second would be to choose the x axis to lie along the major axis of the M_2 tidal ellipse (the single largest tidal component). Both of these are reasonable because they seem to have some relation to the important physics of the problem, and they also do not vary much between the three moorings. The latter comment implies that by choosing only a single axis on which to calculate the stress at all three moorings, we will probably not introduce too much error because the spread between the different axes calculated at each of the three moorings is $\approx 5°$. However, neither the isobath- nor M_2-based axes are capable of reproducing the minor flood/ebb asymmetry that we observe in the tidal current. Here, we mean that the peak flood and the peak ebb current are not aligned at 180° to one another.

We thus choose to use the tidal current averaged over the 1-h time window as the appropriate axis. To be precise, we select a number of velocity–acceleration pairs about which to calculate the Reynolds stresses. Velocities from -90 to $+90$ cm s^{-1} are chosen in 20 cm s^{-1} increments, where the positive tidal current refers to flood, and will further distinguish between when the flow is accelerating (moving toward peak flood/ebb) and when the flow is decelerating (moving toward slack tide). This produces 20 distinct segments, or phases, of the tidal cycle about which to calculate the Reynolds stress. Here we are making a broad assumption that the "phase" of the tidal current can be reduced to an instantaneous measurement of speed and acceleration.

As an example, for a given tidal phase (e.g., $+30$ cm s^{-1} accelerating), we identify in the depth-averaged tidal current at the southern mooring every time at which the tidal current is both flowing at 30 cm s^{-1} and is accelerating. We then calculate the mean tidal vector during 1-h windows centered on these times and as a function of depth. This mean current then sets the direction of the x axis, as a function of depth, that we will use for the Reynolds stress calculation at the south ADCP. For the east and north ADCPs, we then determine, by mapping along isopycnals, with which bin in the south ADCP to compare, and consequently which axis to use in the stress calculation. The depth-averaged current is not strictly barotropic because we exclude part of the water column from the analysis. I disregard the top and bottom 20 m in calculating the depth-averaged current at the south ADCP. This is mainly for consistency with the later eddy viscosity calculations, which will only be performed in the middle of the water column. It also eliminates some difficulties introduced by the bottom Ekman layer around slack tide.

If the axis imposed by the south ADCP on the east and north ADCPs was substantially different from one calculated separately at each mooring, then we might expect difficulty in interpreting the results. This is generally not the case within $\pm 5°$. We could calculate the Reynolds stresses independently at each mooring, but then we shift the analysis problem to the interpretation of the cross-strait shear. Namely, would the stress difference between two moorings be the result of a real stress divergence or is it the fact that we have measured a nondivergent stress on slightly different axes? For the present study we will only compare data when the difference between the axis at each mooring is coaligned to within $\pm 5°$. This check eliminates only about 7% of the total ensembles.

3) CALCULATING SHEAR

To calculate the eddy viscosity we need to have a measure of the lateral shear $\partial U/\partial y$ as a function of depth. The estimates of shear that we obtain by differencing the velocity measurements at two moorings are an estimate of the shear between, not at, the two moorings. However, we optimally want an estimate of the local shear at each mooring. We shall use two sets of shear–stress pairs. The first compares the shear as derived from the south minus the north ADCP, with the stress from the east ADCP. The second calculates the shear assuming that the velocity from the north ADCP goes to zero at the northern sidewall, and comparing this with the stress at the north ADCP. We shall refer to the first method as south–east–north (SEN), and the second as simply north (N). We note that the shear is not based only on the tidal velocity, but also has a component resulting from the slowly varying mean flow. Dynamically, it would be difficult to justify ignoring the mean flow shear, although it is generally quite small compared to the tidal component.

The SEN calculation of shear assumes that the $\partial U^2/$

∂y^2 term is small. It also assumes that $\partial U/\partial x$ is negligible, as does all the work in this paper. We can check the assumption of small curvature by comparing the linearly predicted velocity from the south and north ADCPs with the single Interocean Systems, Inc., S4 current meter on the central temperature chain (T chain north). The predicted versus measured tidal velocities averaged over the 1-h windows used in the stress calculation has a correlation coefficient of 0.92. We are thus confident that the shear from the south–north ADCP pair is appropriate for comparison with the east ADCP.

The assumption that the velocity goes to zero at the northern sidewall is obviously correct, but to assume it does so linearly between the boundary and the north ADCP is probably not. We shall still use this method, but simply recognize that the shear is probably an overestimate in the vicinity of the north ADCP.

b. Reynolds stress acting on the meanders

In this case we consider the meanders plus the long-term estuarine flow as the "mean," and we separately consider how both the tidal currents and the internal wave–eddy field act to transport momentum. The existence of a reasonable spectral gap between the mean and the fluctuations means that we do not need to employ the method of ensemble averaging in these calculations.

An averaging window of six M_2 periods ($\approx$75 h) is chosen for the estuarine Reynolds stress calculation. This window length is the result of wanting to minimize the aliasing of the tidal signals, and yet still distinguish the variations of the mean flow. One might worry about aliasing diurnal components over the six M_2 periods, but you can show that the residual current is less the 0.03 m s^{-1} and hence does not influence observations greatly. The x axis is taken to be the mean of the total estuarine velocity (meander + long term) during a given time window, and again as a function of depth.

Unlike the stress acting on the tide calculation, in this case the axes of orientation calculated at different moorings during the same time window can differ by more than 10°. This makes the calculation of stress divergence troubling, because we are unsure of whether the differences in Reynolds stress between the moorings is the result of physical processes or simply different mean directions. Therefore, we shall calculate Reynolds stresses at each mooring based upon a local axis, and defer the problem of comparison to the discussion.

The shear is a more complex problem for the meanders. As an estimate we shall project the velocities at the east and north moorings onto the direction determined from the south mooring, and calculate the shear as in the tidal case. Thus, the stress and the shear are calculated in slightly different reference frames.

c. Reynolds stress acting on the long-term estuarine flow

In this case we are primarily interested in how the meanders act to transport the momentum of the long-term mean estuarine flow, although we shall also analyze the effects of the tides and the internal wave–eddy field. This is perhaps the easiest example because the axis is simply set by the direction of the depth-varying estuarine current averaged over the whole data record. The remaining velocity components are rotated into the given axis and the whole time series are multiplied to give the stresses. Shear is calculated in a reference frame aligned with the south ADCP mean, as above.

4. Results

a. Effects on the tidal currents

The lateral Reynolds stresses $\overline{uv}$, for the internal wave–eddy band acting on the tides, are plotted in Fig. 4. The figure shows the Reynolds stress as a function of depth for each of the three moorings, and about each of the 20 chosen "phases" of the tide. Each of the individual plots in the figure can be read together from left to right and top to bottom as the tidal current builds from slack toward peak flood, returns to slack, builds to peak ebb, and then returns to the starting point. The plots only include stresses that are significantly different from 0 at an 80% confidence level, where we have assumed that each separate 1-h window about a given velocity–acceleration pair is independent and we have used a chi-squared distribution.

An rms lateral Reynolds stress at the south ADCP is about 0.002 m^2 s^{-2}. It is informative to consider how effective this stress would be in changing the velocity structure of the flow. If we consider that the stress linearly goes to zero between the south ADCP and the steep sidewall to the north (Δy = 1800 m), and we integrate over a 1-h window (Δt = 3600 s), then we find that the change in the velocity field everywhere to the north of the south ADCP is Δu = 0.004 m s^{-1} h^{-1}. Therefore, the stress does not appear capable of effecting a rapid change in the current. Even if we absorbed this stress entirely between the north ADCP and the northern sidewall, a distance of about 350 m, we would only get Δu = 0.02 m s^{-1} h^{-1}. As a comparison the tidal flow can change between +0.80 and −0.80 m s^{-1} in 6 h giving a value of Δu = 0.27 m s^{-1} h^{-1}.

The stress divergence between moorings is similar in magnitude to the total stress. The south and east moor-

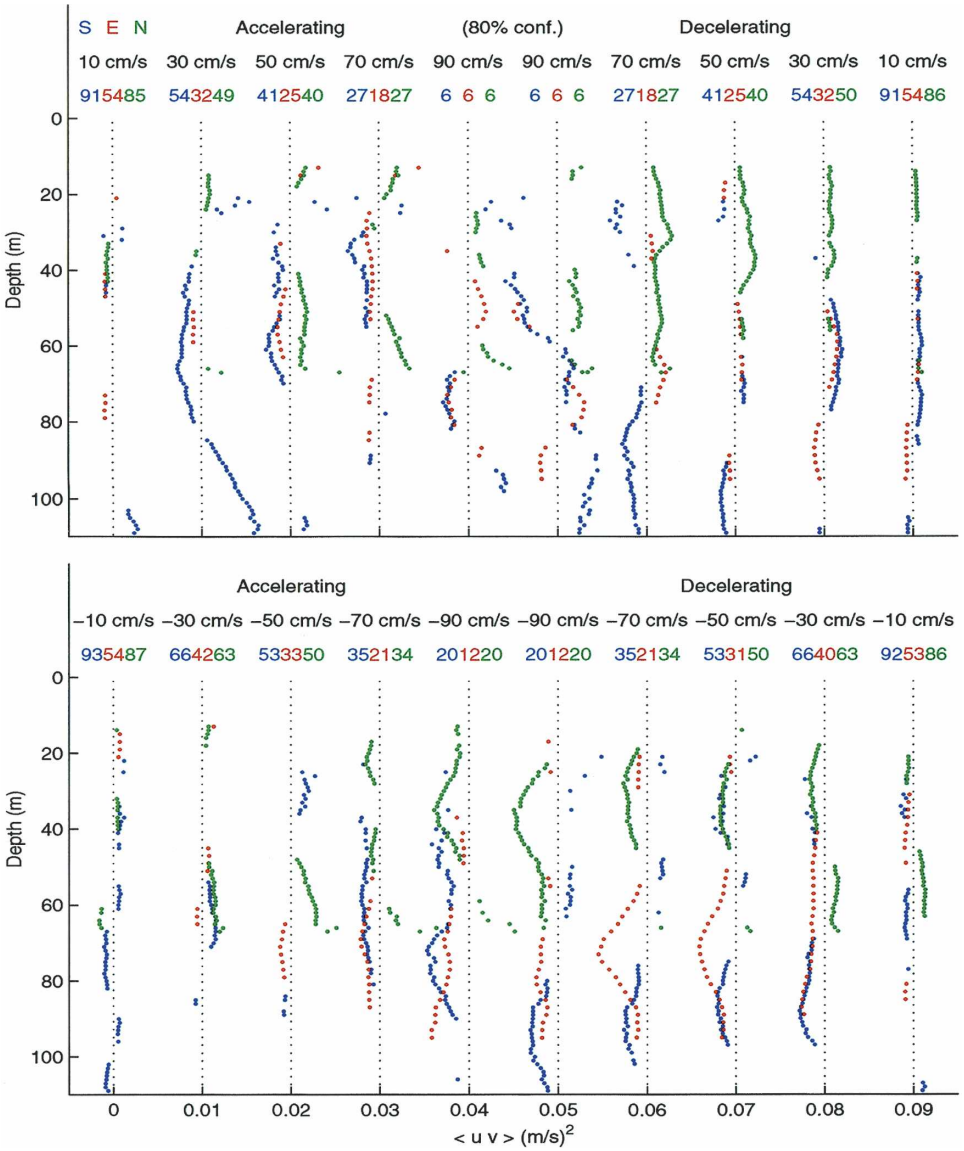

FIG. 4. The $\overline{uv}$ Reynolds stresses acting on a tidal flow "mean." Successive plots represent progressing "phases" of the tide offset by 0.01 $m^2 s^{-2}$ for clarity [(top) flood; (bottom) ebb]. The three moorings are south (blue), east (red), and north (green) ADCP. Only stresses that are significantly different from 0 at an 80% confidence interval are plotted. Colored numbers represent the number of ensembles (degrees of freedom) in each average.

ings generally have stresses that differ by less than 0.001 $m^2 s^{-2}$. This implies a relative acceleration of only 1.2×10^{-6} m s^{-2}. For comparison, the median relative acceleration of the difference in tidal velocities between the south and east moorings for the depth range of 20–70 m is 1.1×10^{-5} m s^{-2}. The stress difference between the east and north moorings is larger, but so too is the relative tidal acceleration. Thus, the internal wave–eddy stress divergence is not an important term in the tidal energy balance. The maximum observed stress divergences, $O(10^{-5}$m $s^{-2})$, correspond to relative changes in velocity of 0.03 m s^{-1} over 40 min (about the time spacing of successive shear and stress plots). However, these tend to coincide with periods of large shear and large relative acceleration of the tidal flow. Let us consider the large stress signature in the east mooring at 80-m depth during the -70 cm s^{-1} decelerating ensemble. If this stress diverged entirely between the east and south moorings it would only represent 25% of the observed tidal acceleration.

We can also examine the implied power per unit length of the strait for the given Reynolds stress, as-

suming $P = \rho H \overline{uv} U_{\text{rms}}$. Using a stress of 0.002 $\text{m}^2\,\text{s}^{-2}$, an average current velocity of $U_{\text{rms}} = 0.45\ \text{m s}^{-1}$, and an average depth between the south ADCP and the sidewall of 90 m implies that between the south ADCP and the northern sidewall we have an average dissipation per unit of length (along strait) of about 80 W m^{-1}. We should note that this is not the total power loss, but only the loss from the internal wave–eddy band. In comparison, this is only 15% of the power lost in the bottom boundary layer [$P = (4/3\pi)\rho C_d U_t^3 Y$], where $C_d = 0.002$ is a drag coefficient, $U_t = 0.8\ \text{m s}^{-1}$ is a tidal velocity, and $Y = 1800$ m is the distance between the sidewall and the south ADCP.

Thus, the majority of energy dissipated in Juan de Fuca Strait is through the turbulent bottom boundary layer. We do not wish to imply that lateral Reynolds stresses are significant in the overall energy budget, at least for the tides. However, we believe that the turbulent tidal dissipation is strongly constrained near the bottom boundary because of the stratification. For the vast majority of the fluid that is outside the immediate vicinity of the boundary, the flow will be determined by a combination of lateral and vertical Reynolds stresses. Ott (2000) showed that the $\overline{u'w'}$ stresses are indistinguishable from zero, except in the internal Ekman layer during neap tides. Instead of revisiting the problem considered by Ott (2000), we have decided to address the lateral transfer issue and see whether there is sufficient transfer to explain the observed cross-strait profiles.

There is a considerable amount of structure in Fig. 4. It is generally encouraging that the stress is both slowly varying in the vertical and between successive "phases" of the tide. It is difficult to interpret individual features without the benefit of the large-scale shear. Consequently, the tidal velocities are shown in Fig. 5. The figure shows the tidal velocities at each mooring rotated into a depth-varying (although only ≈10°) reference frame defined by the south mooring. One first notices that the shear is strongest between the east and north moorings (implying that the shear is larger near the boundary). The average observed velocity difference could exceed 0.4 m s^{-1} between the east and north moorings. Assuming that this is because of a cross-channel, rather than along-channel, gradient leads to a shear of $O(0.0006\ \text{s}^{-1})$. Expressed in terms of the phase of the tidal components, we can observe phase lag gradients away from the boundary of about $1^\circ\ (100\ \text{m})^{-1}$ for both M_2 and K_1 (the two largest components of the tidal current). The east and south moorings have less shear, and it is primarily shear in the lower water column resulting from different bottom depths. Otherwise, the velocities at the two moorings are often within 0.1 m s^{-1} of each other. An exception is during the acceleration toward peak ebb, when the flow field becomes complicated (note that the north and south velocities are both stronger than the east at -0.5 and $-0.7\ \text{m s}^{-1}$ accelerating). We think this may be because of the topographic influence of a downstream irregularity (visible in the inset in Fig. 1).

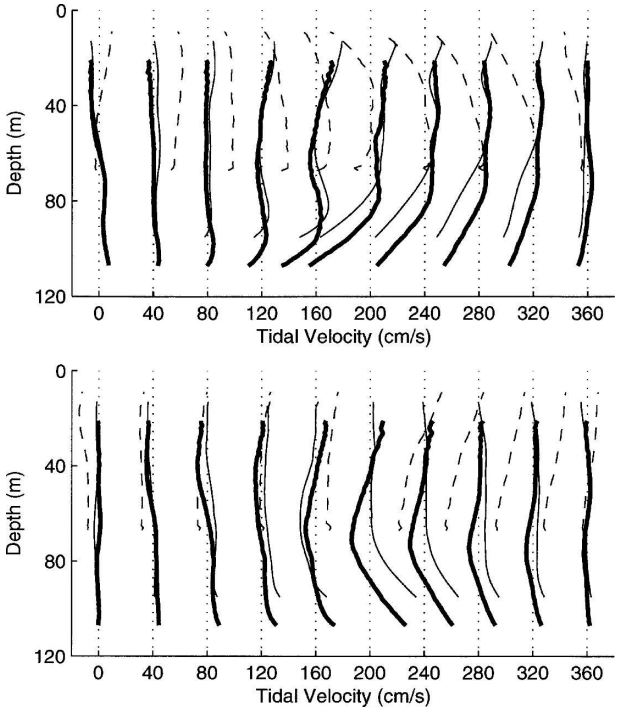

FIG. 5. The ensemble average velocity, relative to the barotropic mean at the south mooring, for the three moorings (south: thick, east: thin, north: dashed) during the tidal phases corresponding to Reynolds stresses in Fig. 4. Successive plots have been offset by 40 cm s^{-1}.

Although the lateral Reynolds stresses are interesting, a horizontal eddy viscosity parameterization would be more useful. Using the measured shear of the mean flow along isopycnals, between the moorings we can calculate an eddy viscosity. Figure 6 shows the shear-versus-stress scatterplots for the two methods discussed in section 3a(3) [SEN (circle) and N (plus)]. The shear-versus-stress plot excludes data from the upper 20 m and the lower 20 m of the water column in order to exclude boundary processes that we are not trying to model. Previous years' observations, including microstructure, have shown that the tidally driven turbulent bottom boundary layer is always less than 20 m thick. Furthermore, within the rest of the water column, we exclude stresses that are not significantly different from zero at an 80% confidence level.

The data are consistent with a down-gradient flux (i.e., the stress and shear are usually of different signs).

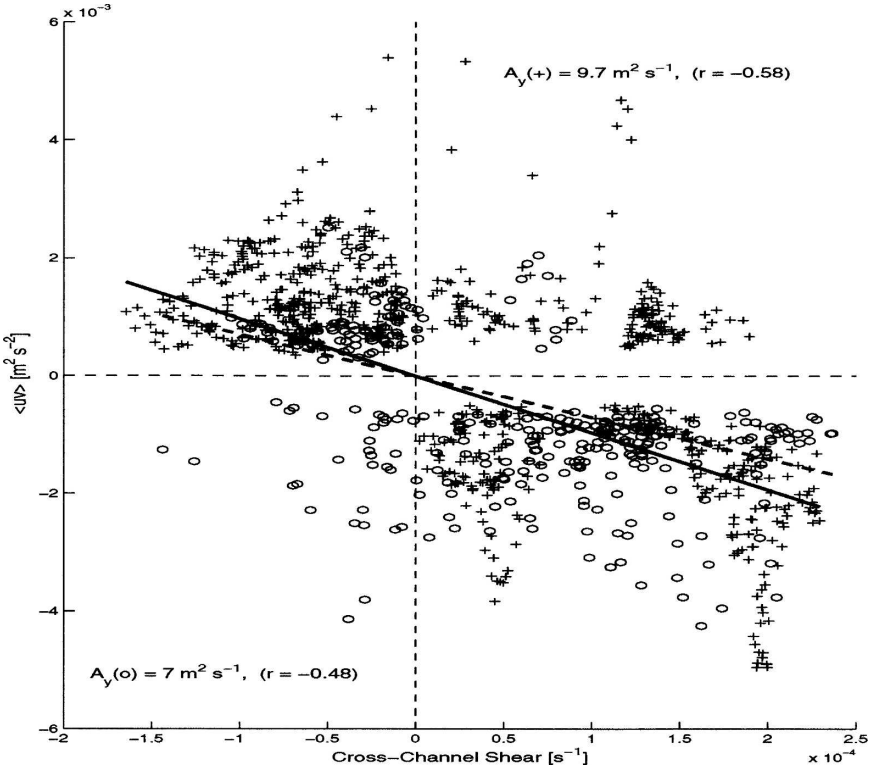

FIG. 6. The shear in the mean tidal flow vs the lateral Reynolds stress for the SEN (circle) and N (plus) methods. Slopes and correlations are as labeled.

We can see that a simple linear least squares fit regression does not appear to adequately fit the data, although it does indicate the rough magnitude of the eddy viscosity. We have examined subsets of the data (e.g., spring versus neap tide and limited depth ranges) with the goal of reducing the scatter in Fig. 6, but have not achieved improvement. All of the chosen subsets have best linear regression fits with slopes in the range of 6–13 $m^2\ s^{-1}$. We thus feel that the mean effect of the internal wave–eddy field might be represented, to first order, by an eddy viscosity of order $O(10\ m^2\ s^{-1})$.

b. *Effects on the slowly varying estuarine flow*

Two sets of fluctuations are projected onto the estuarine flow axis. The first is the internal wave–eddy band and the second is the tidal velocity field. We shall concentrate on the interpretation of the tidal current stresses, but note that the internal wave–eddy field stresses are quite weak and lead to estimates for an eddy viscosity, when scaled by the estuarine shear, that is similar to those in the previous section (i.e., about 10 $m^2\ s^{-1}$).

The tidal Reynolds stresses are plotted in Fig. 7 as a function of depth and yearday. Note that the Reynolds stresses are calculated every 2 days with a six M_2 period window, so that there is some correlation between adjacent 2-day blocks. One of the clear features is the strong spring neap cycle in the Reynolds stress at each of the three moorings. We also note the strong similarity between the north (top) and east (middle) stresses.

However, unlike in the previous section, the tidal stresses do not show any significant correlation with the shear of the estuarine flow. An interpretation of this could be that the estuarine shear is dynamically unimportant when compared to the large shears in the tidal current. However, this is unlikely because the internal wave–eddy stresses in the estuarine reference frame show reasonable correlation with the estuarine shear. It is thus a problem related strictly to the nature of the tidal flow.

The explanation is illustrated in Fig. 8, which shows the measured tidal current Reynolds stresses versus the orientations of the estuarine flow used in the calculations. The tidal currents are largely constrained to flow along the isobaths (for most of the water column below about 30 m), and thus the majority of the lateral Reynolds stress in Fig. 7 is because of the fact that the estuarine flow has an orientation that crosses those iso-

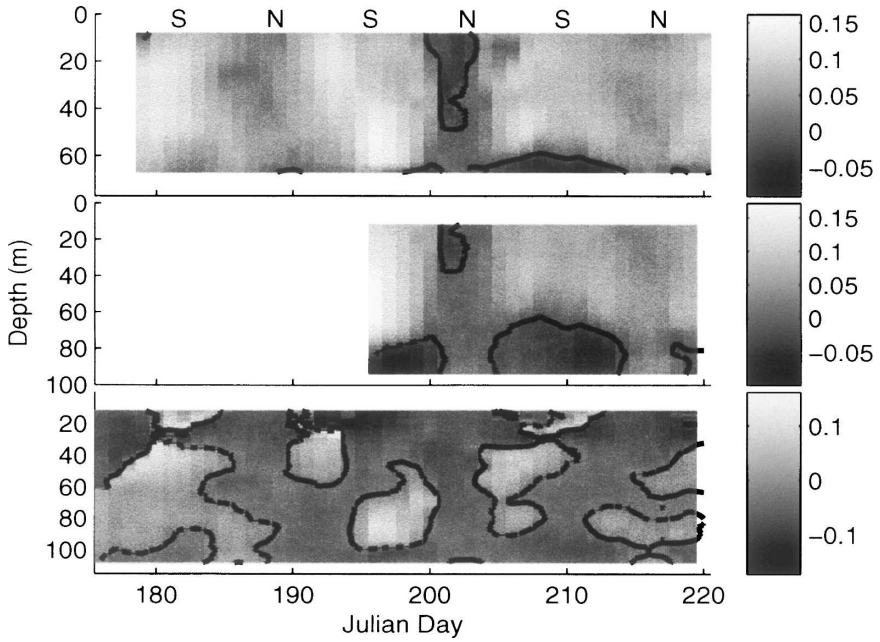

FIG. 7. The tidal Reynolds stress ($cm^2\ s^{-2}$) acting upon an estuarine mean flow for the (top) north, (middle) east, and (bottom) south ADCP. Respectively, S and N along the top of the figure indicate the spring–neap cycle.

baths. Thus, most of the visual difference in the $\overline{uv}$ Reynolds stresses between the moorings in Fig. 7, particularly the south ADCP, is because of changes in the orientation of the estuarine flow between moorings, not gradients in the tidal current. Thus, the problem is because of our inability to choose a suitable reference frame that is appropriate for all three moorings.

As a check we can recalculate the tidal stresses based upon a single axis aligned with the isobaths. The magnitude of the tidal Reynolds stress along isobaths is reduced by almost an order of magnitude (except near the surface). Furthermore, the divergence of this tidal Reynolds stress is everywhere indistinguishable from zero at an 80% confidence interval. We are thus unable to provide any useful quantification of the effect of the tide on the estuarine flow. Any future observations would need a more closely spaced array to eliminate the problems of the curvature of the estuarine field (the

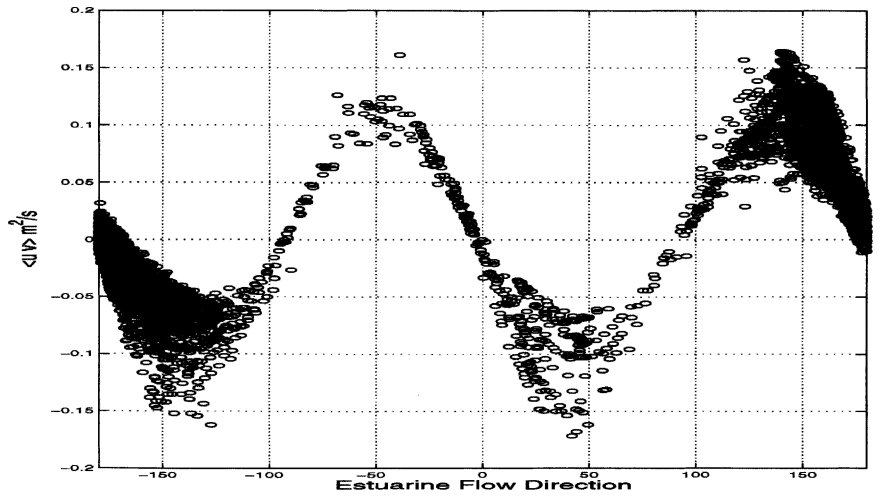

FIG. 8. The tidal current Reynolds stress vs the orientation of the estuarine mean flow used in the calculation of the stress for all three moorings (0° is along-isobath ESE).

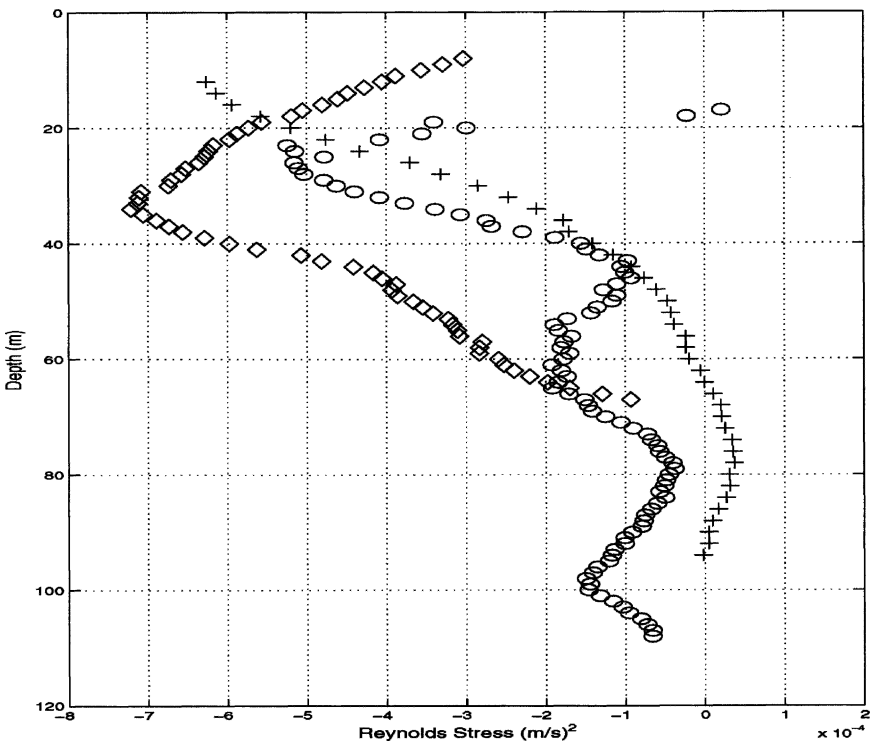

FIG. 9. The lateral Reynolds stress of the meanders projected onto the long-term estuarine flow for the south (circle), east (plus), and north (diamond) ADCPs.

mean), and a longer time series to produce better statistics.

c. *Effects upon the long-term estuarine flow*

In this final case, there are three distinct calculations of Reynolds stress based upon whether we use the internal wave–eddy field, the tidal currents, or the meanders as the "fluctuations." The estuarine mean flow is more closely aligned with the isobaths than the slowly varying mean of the last section, and so the issue of choosing the axis of the mean flow is reduced. The internal wave–eddy field stresses are not significantly different from the results of previous sections and are consistent with an eddy viscosity of $O(10\ \mathrm{m\,s^{-2}})$, although with large error bars. The tidal stresses are not plagued with the problem of a curved mean field, at least to the degree of the last section. However, the stresses are still only weakly divergent so we can obtain no statistically significant results with our time series.

The meander Reynolds stresses in the reference frame of the long-term estuarine mean flow are shown in Fig. 9. We first note that these stresses are quite small, $O(0.0002\ \mathrm{m^2\,s^{-2}})$, although this is not surprising if we consider that the shear in the estuarine flow is also quite weak. They are also all negative, in keeping with an outflowing estuarine flow that is maximal offshore from our moorings. The stresses are weakly correlated (-0.30) with the measured estuarine shear, and a best-fit linear regression line gives an estimated eddy viscosity of $8 \pm 8\ \mathrm{m^2\,s^{-1}}$.

The fact that the stress at the east mooring is smaller in magnitude than either the south or north moorings is unexpected. Qualitatively, the stress divergence between the south and east moorings implies that the mean flow should be accelerating out to sea (i.e., increasing in magnitude). Thus, the meanders appear to be reducing the shear between the south and east moorings. Conversely, the stress difference between the east (and south) mooring and the north mooring imply that $dU/dt > 0$. Therefore, the flow at the north mooring should be decelerating. Coupled with the acceleration further away from the boundary, this implies that the meanders are intensifying the shear at some central location. This is interesting because it implies local regions of up-gradient flux.

5. Discussion

The lateral Reynolds stresses affecting the profile of the currents near the sides of Juan de Fuca Strait were

successfully measured. More importantly, the array measurements represent the first observations of Reynolds stress differences and horizontal eddy viscosity on the medium-scale separation, $O(1\text{ km})$, of our instrument array.

The tidal current, which exhibits a fairly slablike profile, is acted upon by the stress divergence of the internal wave–eddy field. The observed stress differences between the ADCP moorings show reasonable correlation with the observed cross-strait shear. The inferred eddy viscosity for the internal wave–eddy field is estimated to be $\approx 10\ \text{m}^2\ \text{s}^{-1}$.

The total estuarine flow (meanders plus long-term mean) is acted upon by both the internal wave–eddy field and the tidal currents. The internal wave–eddy field acts in a very similar way to the previous case, and is consistent with an eddy viscosity of $O(10\ \text{m}^2\ \text{s}^{-1})$. However, unlike the case of the tidal flow, which reverses direction, and hence shear, every 6 h, the total estuarine flow has shear that is consistently positive near the moorings. Thus, the net effect of the internal wave–eddy field is always to decelerate the flow. Although the stresses are weak, they can produce measurable change when integrated over many days.

The tidal currents can exhibit a large Reynolds stress for an axis that is oriented at an angle to the mean isobaths. This tidal stress is substantially reduced, and at best is weakly divergent, when calculated in an isobath reference frame. This conclusion should be reexamined with a more detailed experiment that can better resolve both the structure of the estuarine flow and the tidal currents very close to the boundary.

The long-term estuarine flow is acted upon by three components: the internal wave–eddy field, the tidal currents, and also the slow meanders about the long-term mean state. These meanders produce very small stresses, but as in the previous case, the effect when integrated over time can be important because of the consistent sign of the shear in the long-term estuarine flow. These meanders impose an additional eddy viscosity of $8 \pm 8\ \text{m}^2\ \text{s}^{-1}$. Again a longer-term deployment with better spatial resolution could help to improve this estimate.

Returning to our initial observation that the tidal flow is largely slablike while the estuarine flow is markedly curved, we ask the question of whether our results agree with this observation. The slablike tidal current is subject to the effects of internal waves and eddies that have a net effect of imposing an eddy viscosity of $O(10\ \text{m}^2\ \text{s}^{-1})$. The estuarine flow is also subject to this viscosity plus the effect of meanders, giving a total viscosity of $O(10\ \text{m}^2\ \text{s}^{-1})$. The two sources of viscosity are not the most important factor in explaining the difference in observed cross-strait profiles, instead it is the period over which this viscosity acts that matters. In the case of the tidal flow, the velocity and the shear reverse every 6 h. Thus the eddy viscosity has little time to act upon the flow field. By contrast, the estuarine flow is consistently in one direction and the eddy viscosity acts progressively upon the flow during the time it takes to transit the length of Juan de Fuca Strait, about 10 days. If we assume that all of the stress divergence between the south ADCP and the northern sidewall goes into changing the velocity of the estuarine flow and integrate over 10 days, we find that the observations result in a net deceleration of the estuarine flow of between 0.15 and $0.2\ \text{m}\ \text{s}^{-1}$. This represents an order one effect on the estuarine flow.

Out of interest, we can examine the expected boundary layer width given the above eddy viscosities. The width of a growing boundary layer can be written as $w = \sqrt{A_H x/U}$. Assuming an rms velocity of $U = 0.5\ \text{m}\ \text{s}^{-1}$ and using the fact that the moorings are located about 50 km from either end of the strait, the width is $w = 1$ km. If instead we use a scaling related to the tidal flow $w = \sqrt{A_H/\omega_{M2}}$, we find that $w = 250$ m.

It should be noted that the eddy viscosities we obtain from these observations are not universally applicable numbers. Instead, the eddy viscosity must relate to some formula that attempts to incorporate the physics of the problem. For instance, we might suspect that the tidal input of energy into the system is important because it generates the waves and eddies that do the mixing. If we believe that the mixing is entirely because of eddies stirring the near-shore water, then an appropriate formula might be $\kappa_H = cUL$, where U and L are the eddy speed and width. The eddies are generated near the shore by the tidal flow, and so we might assume that the above U and L are themselves related to the tidal velocity $U_t \approx 0.8\ \text{m}\ \text{s}^{-1}$, and either the dominant scale of the bathymetry $L_b \approx 2$ km or the length of a tidal excursion $L_t \approx 8$ km. This gives a rough value for the constant c of between 0.5 and 6. In practice, measurements from several different locations will have to be synthesized to achieve a better parameterization.

Furthermore, not all models employ a constant eddy viscosity term to parameterize the subgrid-scale horizontal eddy viscosity. Masson and Cummins (1999, 2000) use the common Smagorinsky approach to model subtidal flow around Vancouver Island. Using their choice of nondimensional constant with the observed subtidal strain leads to an eddy viscosities of $O(20\ \text{m}^2\ \text{s}^{-1})$. However, the choice of nondimensional constant is clearly frequency dependent, because the observed tidal strains are larger and thus for a fixed constant would imply large eddy viscosities.

Acknowledgments. This work was funded through grants from the Office of Naval Research. The ship time was paid for with funding from the Natural Sciences and Engineering Research Council (Canada) and carried out aboard the CCGS *Vector*. The mooring work was organized and supervised by Dr. Richard Dewey. Numerous draft revisions have been thoroughly read and digested by my Ph.D. supervisor, Dr. Chris Garrett. The author also thanks two anonymous reviewers for greatly improving the clarity of the paper.

REFERENCES

Colbo, K. M., 2002: Mixing processes near boundaries. Ph.D. thesis, University of Victoria, 212 pp.

Dewey, R., 1999: Mooring design and dynamics—A Matlab package for designing and analyzing oceanographic moorings. *Marine Models,* **1,** 103–157.

Edwards, K. A., P. MacCready, J. N. Moum, G. Pawlak, J. Klymak, and A. Perlin, 2004: Form drag and mixing due to tidal flow past a sharp point. *J. Phys. Oceanogr.,* **34,** 1297–1312.

Foreman, M. G. G., 1978: Manual for tidal currents analysis and prediction. Pacific Marine Science Rep. 78-6, 57 pp. (Revised 1996.)

——, R. A. Walters, R. F. Henry, C. P. Keller, and A. G. Dolling, 1995: A tidal model for eastern Juan-de-Fuca Strait and the southern Strait of Georgia. *J. Geophys. Res.,* **100,** 721–740.

Labrecque, A., R. Thomson, M. Stacey, and J. Buckley, 1994: Residual currents in Juan de Fuca Strait. *Atmos.–Ocean,* **32,** 375–394.

Masson, D., and P. F. Cummins, 1999: Numerical simulation of a buoyancy-driven coastal countercurrent off Vancouver Island. *J. Phys. Oceanogr.,* **29,** 418–435.

——, and ——, 2000: Fortnightly modulation of the estuarine circulation in Juan de Fuca Strait. *J. Mar. Res.,* **58,** 439–463.

Ott, M. W., 2000: Mixing and secondary circulation in Juan de Fuca Strait. Ph.D. thesis, University of Victoria, 162 pp.

Sundermeyer, M. A., and J. R. Ledwell, 2001: Lateral dispersion over the continental shelf: Analysis of dye-release experiments. *J. Geophys. Res.,* **106,** 9603–9621.

Thorpe, S. A., 1992: The generation of internal waves by flow over the rough topography of a continental slope. *Proc. Roy. Soc. London,* **439A,** 115–130.